CONCRETE LIBRARY OF JSCE NO. 29, JUNE 1997

COMPUTATIONAL MODEL FOR REINFORCING BAR EMBEDDED IN CONCRETE UNDER COMBINED AXIAL PULLOUT AND TRANSVERSE DISPLACEMENT

(Reprinted from Journal of Materials, Concrete Structures and Pavements, No.538/V-31, May, 1996)

Koichi MAEKAWA

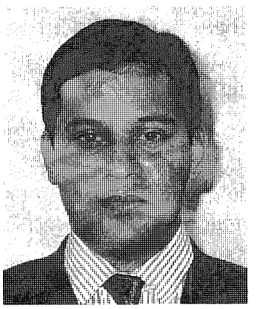

Juneid QURESHI

An enhanced computational model for the prediction of reinforcing bar behavior under generic axial pullout and transverse displacement conditions is presented. Based on the compatibility relationship between transverse displacement and curvature induced in the embedded bar, localized bar phenomenon close to the interface are formulated. This formulation makes it possible to express the reduced pullout stiffness of embedded bars which is observed under combined axial pullout and transverse dowel action.

Keywords: *Bond, dowel action, pullout, reinforcement, constitutive law*

K. Maekawa is Professor in the Department of Civil Engineering at the University of Tokyo. His research interests cover reinforced concrete mechanics, computational approaches to the seismic behavior of reinforced concrete-soil systems and the thermodynamic solid physics of cement-based composites. He is active in JSCE committees and has been involved in outlining performance based design of concrete structures in the last few years. The integration of mechanics of solids with thermo-physical requirement is his current main concern, and he is seeking for universal durability performance evaluation system.

J. Qureshi earned his Master degree from Asian Institute of Technology and his doctorate degree from University of Tokyo in 1993. His subject of research at the Department of Civil Engineering was the integration of bond and stress transfer across a concrete crack for establishing an universal RC joint interface element. His engineering interests range from the fundamentals of reinforced concrete to practical design of buildings and infrastructures. He is Structural Engineer in Meinhardt Pte Ltd. in Singapore.

1. INTRODUCTION

There are several constitutive laws which can be combined to formulate plate and joint models for smeared and discrete crack elements in FEM applications. In general, these constitutive laws have been verified under simplified loading conditions, and their applicability under generic conditions needs to be checked. The relation between bond stress-slip-strain has been formulated [2] by treating the reinforcement in concrete as a one-dimensional cord. This consideration is valid for a single-mode deformational path in which the reinforcement is subjected to axial deformation only. However, when deformational paths are of a mixed-mode nature, i.e. axial pullout coupled with transverse displacement, the applicability of this model is invalidated in terms of a reduction in axial stiffness and mean yield strength of the reinforcement due to a zone of localized yielding in the reinforcement close to the crack plane, as detailed elsewhere[16]. The shear capacity of a crack plane, which might govern the ultimate load under specific structural conditions, is therefore not governed by the axial stiffness and strength represented by bare steel bars under uniaxial deformation, but by that of the coupled interaction between longitudinal and transverse displacement. This depends on the equilibrium and compatibility requirements of a crack plane, and cannot be ignored when an RC joint plane has small roughness and/or heavy reinforcement ratio[5].

In this paper, an enhanced computational model for the prediction of reinforcing bar behavior under the generic conditions of axial pullout and transverse displacement is presented. It is based on the relationship between transverse displacement and the maximum curvature induced in the embedded bar, along with a consideration of localized phenomena for a bar close to a crack and interface.

2. REINFORCING BAR PULLOUT COUPLED WITH TRANSVERSE SHEAR

A number of previous studies have developed separate constitutive models for steel and concrete components, but most have been verified under simplified and idealized loading conditions. Reinforcement has been modeled by separately considering the two actions of axial pullout and transverse shear, and then superposing these behaviors. Models of reinforcement under uniaxial pullout have been proposed by several researchers, who have established microscopic and macroscopic bond models[2),7),8)]. Shima et al.[2)] formulated a constitutive model for bond stress, strain, and axial slip considering both microscopic and macroscopic aspects of the bond. This model become the framework for modifications leading to this proposed enhanced model for embedded bars under generic displacement paths.

Results of tests on embedded bars under loads transverse to the bar axis have been utilized by several researchers to predict the maximum dowel capacity and transverse load - displacement relationships of reinforcement [4),6)]. Nonlinear "beam on elastic foundation" models with variable subgrade stiffness have been proposed, but these are limited to reinforcement subjected to transverse loads only; consideration of bar plasticity or additional damage build-up in concrete -- due to radial bond micro cracks originating from the coupled axial loads -- has been absent, although these are the conditions which reinforcement is subjected to in most RC interfaces.

In the past, the shear capacity of RC interfaces[5)] has been predicted by the superposition of the bar axial bond stress-strain-slip model[2)] with a plain concrete stress transfer model[3)] . However, such predictions are unsatisfactory [16)] , usually resulting in over-estimation of capacity and associated shear displacement when the crack planes are heavily reinforced, even while neglecting the dowel contribution of reinforcing bars. Since the bond stress-slip-strain model proposed in (2) was formulated under pure tensile conditions, it was presumed that one of the major reasons for this errors estimating shear capacity is the incorrect model for estimating confinement provided by the axial stiffness and strength of the reinforcement under the coupled action of crack opening and transverse shear.

To investigate embedded bar behavior when subject to a coupled displacement path, pure shear loading was adopted in beam-type specimens as shown in **Fig.1**[16)]. The shear displacement and associated dilatancy of the shear plane simulates the generic loading path for the embedded bar. By varying either the confining force on the interface, the reinforcement ratio, or the shear plane geometry, different displacement paths were studied for the targeted reinforcing bar. Test results, which form the basis of this study, showed a significant fall in bar axial stiffness and strength under these coupled displacement paths as compared with pure uniaxial traction [2)] . Details of the test setup and results can be found in the accompanying study (16).

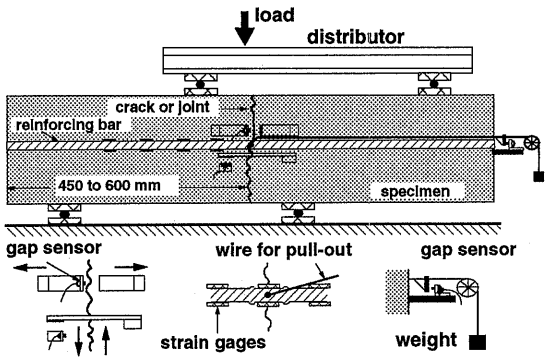

Fig.1 Experimental set-up, instrumentation, and loading[16)]

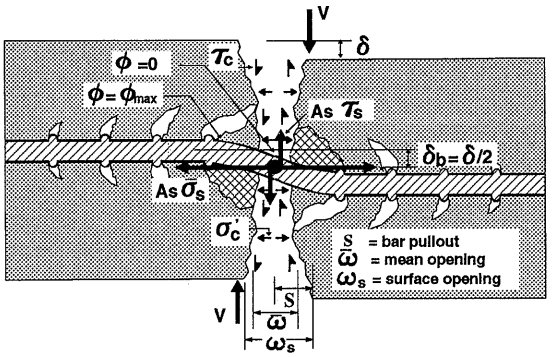

Fig.2 Embedded bar subjected to coupled displacement path

3. ANALYTICAL MODELING

(1) Mechanical behavior of embedded bar across interface

In a reinforced concrete interface subjected to a shear stress defined as τ_c, a shear displacement, δ, is produced. Also, because the crack surfaces ride over each other, a normal compressive stress, σ'_c, is induced along with an associated normal displacement denoted by ω (crack dilatancy). This normal displacement causes a pullout force on the confining embedded steel reinforcement at the interface, S, thereby inducing an axial strain $\bar{\varepsilon}_s$. The shear displacement also produces a zone of curvature ϕ along the reinforcement close to the interface, at the location where the induced curvature reaches its maximum, $\phi_{max.}$ Due to symmetry, the curvature value is zero at the interface and thus the mean confining steel stress, $\bar{\sigma}_s$, at this location is determined only by $\bar{\varepsilon}_s$ induced by the bar pullout force.

However, within the curvature affected zone, $\bar{\sigma}_s$ is influenced by both the pullout force and shear slip at the interface owing to the steel's three-dimensional extent. These parameters, which define the deformational and mechanical characteristics of a RC interface, are shown in **Fig.2;** here the crack width and shear slip are magnified to clearly indicate the notation. To determine the load deformation relationship and the capacity of the interface, a formulation of embedded bar axial stress under the action of normal and transverse displacement is essential.

(2) Review of bond stress-strain-axial slip model

Shima et al.[2)] proposed a bond stress-strain-axial slip model for reinforcement under uniaxial pullout rods conditions. The differences in bond-slip relations obtained from pullout tests of long and short embedded rods and from axial tension tests were expressed by using a unique bond stress-slip-strain relationship, in which the bond stress is formulated as a function of strain multiplied by a function of slip. The latter is defined as the bond stress when the bar strain is zero. The constitutive law for bond stress is given by,

$$\begin{aligned} \tau_b(\bar{\varepsilon}_s, s) &= \tau_{bo}(s)\, g(\bar{\varepsilon}_s) \\ \tau_{bo} &= f_c'\, k\{\ln(1+5s)\}^c \\ g(\bar{\varepsilon}_s) &= (1+10^5 \bar{\varepsilon}_s)^{-1} \end{aligned} \tag{1}$$

where τ_b is the bond stress, τ_{bo} is the intrinsic bond stress when the bar strain is zero, g is a function depending on bar axial mean strain, f'_c is the compressive strength of the concrete, s is non dimensional slip (= 1000 S/D), S is slip, D is bar diameter, and k and c are constants of value 0.73 and 3, respectively.

The pullout case of interest in the enhanced modeling of the bar and the boundary conditions are shown in **Fig.3.** The equilibrium between bond stress and mean axial stress is defined by,

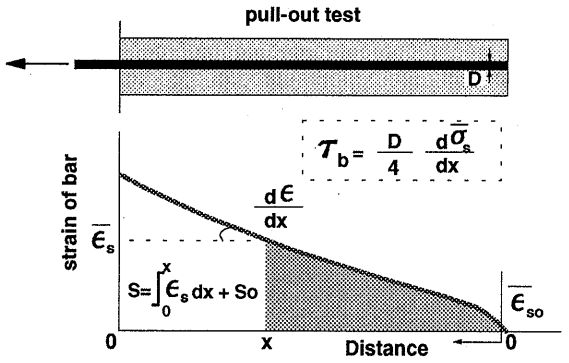

Fig.3 Definitions of local bond stress and slip in model by Shima et al.[2)]

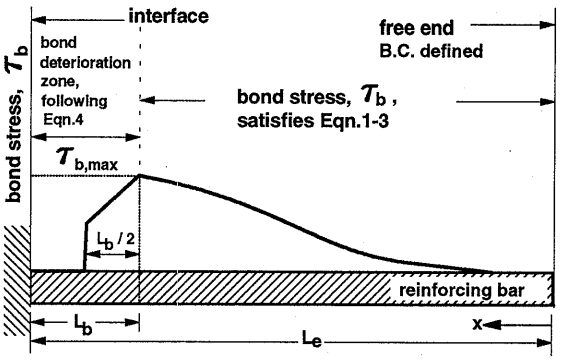

Fig.4 Bond stress profile along embedded bar with deterioration of bond close to the interface

$$\tau_b = \left(\frac{D}{4}\right)\frac{d\bar{\sigma}_s}{dx} \tag{2}$$

The compatibility between axial slip and axial strain is given by,

$$S(x) = \int_o^x \bar{\varepsilon}_s \, dx + S_o \tag{3}$$

where S_o is the slip of the bar at the free end.

This bond stress-slip-strain model, which takes into account the effects of bar diameter and concrete strength and which is applicable to both the elastic and plastic ranges independent of steel properties, is adopted as the framework on which modifications for the proposed model are introduced.

It has been reported[16)] that two new features of bar behavior were witnessed experimentally: (1) non-uniformity in the distribution of mean strain close to the crack plane, with some extreme fibers in the reinforcement reaching plastic strains in some particular locations although the mean strain at the interface and other points away from the interface remains elastic even up to the ultimate load; and (2) the curvature induced in the bar due to the transverse shear displacement is also non-uniform with zero curvature at, and up to some distance from, the interface. The mean stresses in the reinforcement close to the crack plane, however, are rather uniform.

(3) Proposals for model considering localized effects

In view of the 'localized effects' of bar behavior close to the interface, two basic proposals are postulated taking into consideration the different stresses and deformational fields to which the bar is subjected near the interface.

a) Zone of Bond Deterioration:

In the original pullout tests carried out to formulate the bond stress-strain-axial slip model, an unbonded zone was placed near the loaded surface to ensure uniform bonding over the whole extent of the reinforcement[2)]. However, bond performance near the real interface is easily lost due to the splitting and crushing of concrete around the bar. In order to consider this effect, a 'Bond Deterioration Zone' is defined as L_b, the range of which is a function of bar diameter, i.e. $L_b = L_b(D)$. In the computational model, L_b is taken as '5D', but not less than the 'Curvature Influenced Zone', which is discussed later. The degradation in bond stress within this zone is given by a simple bi-linear function as expressed below.

$$\begin{aligned} &\tau_b(x) = \tau_{b,\max} - \frac{\tau_{b,\max}}{L_b}\{x-(L_e-L_b)\}, \qquad (L_e - L_b \le x \le L_e - L_b/2) \\ &\tau_b(x) = 0 \quad (L_e - L_b/2 \le x \le L_e) \end{aligned} \tag{4}$$

where $\tau_{b,max}$ is the maximum bond stress attained at the origin of L_b. L_e is the bar embedded length of the bar. The bond stress profile along the embedded length, including the newly introduced profile representing the concept of a bond deterioration zone, is shown in **Fig.4**.

The concept of a bond deterioration zone is introduced by considering a linear degradation of bond stress from the origin of the deterioration zone to the crack surface[12]. The profile adopted here, where the bond stress drops to zero after some finite distance in the deterioration zone, represents the locus from which radial bond micro-cracks reach the surface of the interface plane and τ_b decreases rapidly. It should be noted, however, that as long as a bond deterioration zone of appropriate size is considered, the profile of degradation is not a highly sensitive parameter.

In the present model, the strain profile is integrated over the entire embedded length, L_e, to find the loaded end slip. Within the Bond Deterioration Zone, L_b, the mean axial strain, $\bar{\varepsilon}_s(x)$, is a function of mean axial stress, $\bar{\sigma}_s(x)$, which in turn is computed from the pre-defined bond stress profile, $\tau_b(x)$, within the zone, i.e.,

$$S = \int_0^{L_e - L_b} \bar{\varepsilon}_s(x)dx + \int_{L_e - L_b}^{L_e} \bar{\varepsilon}_s(\tau_b(x))dx + S_o \tag{5}$$

Thus, the quantitative effect of bond deterioration on additional bar pullout can be obtained, irrespective of the embedded length.

b) Zone of Curvature Influence: To consider the effect of localized curvature of the bar close to the shear plane, the concept of a 'Curvature Influenced Zone', L_c, is introduced. In the tests, L_c was observed to be between '4D' and '5D' initially, with a small increase of '1D' to '2D' as the load increased, as shown in **Fig.5**. In the model, the initial zone size, L_c ($=L_{co}$), at small displacements (when both materials can be considered to behave elastically), is idealized by considering the bar behavior analogous to a beam on an elastic foundation (BEF). This gives,

$$q = -(kD)\delta_b \tag{6}$$

where δ_b is the local downward deflection of the supporting concrete foundation under the bar, q is the downward (and -q the upward) force per unit length of the bar, and k is the foundation modulus taken as constant over the bar diameter, D. Using the classical beam equation, and substituting Eq.(6), we have,

$$\frac{d^4\delta_b}{dx^4} + \frac{(kD)}{E_s I_b}\delta_b = \frac{p'}{E_s I_b} \tag{7}$$

where p' is any external linear downward load acting on the bar, and E_s and I_b are the elastic modulus and moment of inertia of the bar section, respectively. Since the embedded bar is not subject to any external linear load, the 'reduced' (p'=0) general solution to the above equation is therefore,

$$\begin{aligned} \delta_b &= \exp(\beta x)(C_1 \cos\beta x + C_2 \sin\beta x) \\ &+ \exp(-\beta x)(C_3 \cos\beta x + C_4 \sin\beta x) \\ \text{where} \quad \beta &= \sqrt[4]{\frac{kD}{4 E_s I_b}} \end{aligned} \tag{8}$$

If the origin of x is taken to be the shear plane interface and defined as x', the constants of integration can be worked out from the boundary conditions at the two ends for an embedded bar of semi-infinite length subjected to only an external shear force V at the interface with zero bending moment M(=0). That is,

$$\begin{aligned} At \;\; x' \to \infty, \;\; & \delta_b = 0 \;\; (C_1 = C_2 = 0) \\ At \;\; x' = 0, \;\; & E_s I_b \delta''_b = M = 0 \\ and \;\; & E_s I_b \delta'''_b = V \end{aligned} \tag{9}$$

Solution of this differential equation yields,

$$E_s I_b \delta_b{}''' = V\{\exp(-\beta x')(\cos\beta x' - \sin\beta x')\} \tag{10}$$

Then, the location of the maximum bending moment, and consequently of maximum curvature, x_c', from the interface, is given by,

$$x_{c'} = \frac{\pi}{4}\sqrt[4]{\frac{4E_s I_b}{kD}} \quad at\ E_s I_b\ \delta''' = 0 \tag{11}$$

For the model, L_{co} is taken to be three times the size of the distance to the point of the maximum bending moment, as would be derived from BEF analogy, to give,

$$L_{co} = \frac{3\pi}{4}\sqrt[4]{\frac{4E_s I_b}{kD}} \tag{12}$$

$$where \left[k = \frac{150 f_c'}{D} \left(\frac{MPa}{mm^3}\right) \right]$$

The definitions of x'_c and L_{co} are illustrated in **Fig.5**, along with a schematic representation of variations in the curvature profile as seen in the test results.

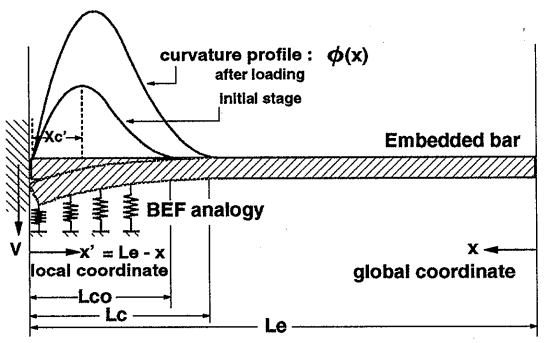

Fig.5 Location of maximum bending moment and size of curvature zone

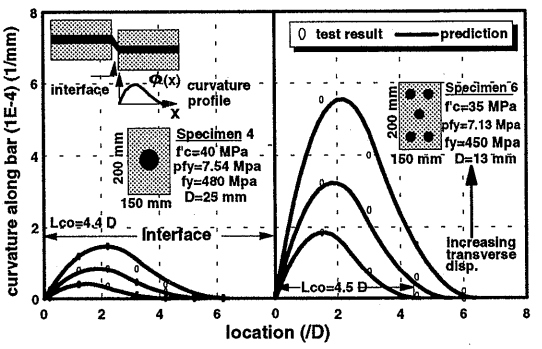

Fig.6 Test [16] and predicted profile of curvature distribution along bar axis for a typical specimen
p : reinforcement ratio; fy : yield strength

Here it is important to mention the equivalence and differences between the 'curvature-distribution model' and the 'beam on elastic/inelastic foundation model'. It is possible to start with an inelastic reaction model of the concrete foundation, based on which the curvature profile may be derived. In this case, however, the model is very complex and it becomes necessary to consider variations in bearing reaction along the bar axis at different distances from the interface. These cannot be directly measured through an experimental approach, because there is a concrete surface in contact with the opposite side. Furthermore, since the bearing reaction in the supporting concrete develops from the transverse displacement of the embedded bar, relaxation of the contact pressure due to localized yielding of the bar is difficult to model using this approach.

For these reasons, it was decided to begin computations with a profile pattern of the curvature and the size of its influence zone; these can be directly observed in experiments. This approach is similar to the method used by Izumo et al.[10] to model the tension stiffening behavior of reinforced concrete based on a trigonometric function for the tensile stress profile of the main reinforcing bars. The main advantage of adopting this approach is that reliable experimental data -- not microscopic data but macroscopic data with a lose association with the microscopic fundamentals of a transversely supported reinforcing bar -- form the basis for the model.

The BEF analogy acts as the basis for computing the location of the initial maximum bending moment based on the parameters which influence the curvature zone, since there are no available test results of curvature profiles

for a wide range of variation of these parameters. For the reasons detailed above, however, the BEF analogy cannot be considered reliable in the later stages of bar pullout and shear displacement, since both the embedded bar and the supporting concrete behave nonlinearly. As seen in the test results[16], there is a small shift in the curvature influenced zone with increased shear displacements. The mechanical meaning of this shift is that it reflects inelasticity in the reaction spring properties, because the inelasticity relaxes the moment localization. Changes in the influence zone are basically associated with local crushing or high inelasticity of the reacting concrete near the interface. This gradual softening in the supporting concrete due to increasing bar shear displacement, δ_b, and radial micro bond cracking due to bar pullout, S, is modeled by considering an increase in L_c, as a function of L_{co} and introducing a non-dimensional damage build-up parameter, DI, as expressed below.

$$
\begin{aligned}
DI &= (1 + 150\,S / D)\,\delta_b / D \\
L_c &= L_{co} \qquad (for\ DI \le 0.02) \\
L_c &= L_{co}\{1 + 3(DI - 0.02)^{0.8}\} \\
&\quad (for\ DI > 0.02)
\end{aligned}
\tag{13}
$$

The shape of the curvature distribution, $\phi(x)$, within L_c is modeled by a skewed parabola. This conforms well with the curvature profile seen in test results[16], as shown for a typical specimen in **Fig.6**, and is expressed as below.

$$
\begin{aligned}
\phi(x) &= \frac{3\phi_{max}[x - (L_e - L_c)]^2}{L_c^2} \\
&for \quad L_e - L_c \le x < L_e - L_c / 2 \\
\phi(x) &= -3\frac{\phi_{max}}{L_c^2}[3\{x - (L_e - L_c / 2)\}^2 \\
&\quad - L_c\{x - (L_e - 3L_c / 4)\}] \\
&for \quad L_e - L_c / 2 < x \le L_e
\end{aligned}
\tag{14}
$$

A comparison of variations in L_c with test results for a few typical specimens is shown in **Fig.7**.

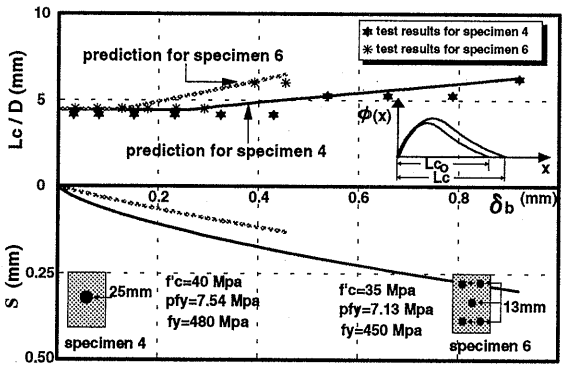

Fig.7 Comparison of predicted and test results of variations in curvature influenced zone under coupled displacement path for typical specimens

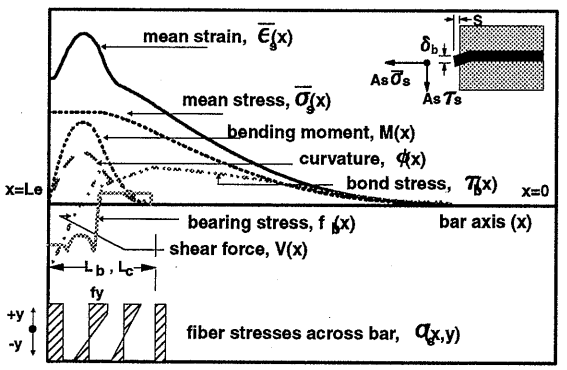

Fig.8 Graphical distribution profiles of typical computed parameters

The size of the curvature influenced zone and the shape of the curvature profile are modeled primarily to reproduce the curvature profiles observed in test results. The expression for underlying concrete subgrade stiffness, k, is within the range of values of k adopted in the literature by different researchers, as summarized by Poli et al.[4]. Equation (12), derived from the BEF analogy, is a convenient way to model the zone size based on all relevant influencing parameters, i.e. bar size, and concrete and steel stiffnesses. Predictions of axial and transverse bar stresses for tests conducted for this study along with data available in the literature, as will be shown in a later section, validate this modeling of subgrade stiffness along with the zone size and shape for a

sufficiently wide range of influencing parameters. A direct verification of zone size and shape against test data from experiments conducted for this study was also carried out, as shown in **Fig.6** and **Fig.7**.

(4) Compatibility between bar transverse displacement and curvature distribution

Using the assumptions of classical beam theory, the compatibility conditions require that the sum of the double integral of the curvature distribution, $\phi(x)$, and the integral of the transverse shear deformation, $\gamma(x)$, along the bar axis must equal the displacement of the bar normal to that axis, $\delta_b(x)$. To satisfy boundary and continuity conditions, we have,

$$\begin{aligned} \delta_b &= \iint_{L_c} \phi(x)\, dx + \delta_{bs} \\ \delta_{bs} &= \int_{L_e} \gamma(x)\, dx \end{aligned} \tag{15}$$

where L_c indicates the size of the curvature influenced zone. Integrating over this zone gives the transverse displacement of the bar at the interface, which by compatibility becomes half of the shear displacement of the interface, δ, as shown in **Fig.2**.

This geometric compatibility, which holds true irrespective of bar elastic and plastic behavior is one of the key relations in the computational model. Once the bar transverse displacement, δ_b, is known, the curvature profile, $\phi(x)$, and the axial and transverse stresses in the embedded bar can be computed under the coupled action of axial pullout and transverse displacement.

The force system acting on the embedded bar due to the displacement path at the interface, which will be discussed in detail in the next section, causes insignificant shear deformation of the bar at the interface. The imposed boundary conditions at the ends of the curvature influenced zone, i.e. the origin and the interface mean that the bending moment must be zero. The profile of the shear force acting on the bar therefore follows a positive and negative contour. Under elastic conditions, the transverse bar displacement due to shear deformation only, δ_{bs}, can be expressed as,

$$\delta_{bs} = \frac{\alpha}{GA_s}\int_{L_e} V(x)dx = \frac{\alpha}{GA_s}\int_{L_e} dM \tag{16}$$

where, α is a shape factor which is a function of the shear stress distribution in the cross section, G is the shear modulus of elasticity and A_s is the cross-sectional area.

As a result of the boundary conditions, as mentioned above, the difference in bending moment across L_c must be zero. Therefore, shear deformation under elastic conditions can be considered non-existent. After localized yielding of the outer fibers of the bar due to curvature, plasticity develops on both sides of the maximum curvature location, i.e. it encompasses both positive and negative shear force regions, and additional shear deformations at the interface location caused by loss of shear rigidity close to the interface are also mostly balanced between these two regions. In view of this behavior, in general, the effects of shear displacement are not considered in the computational model. Verification against test results also indicates that by considering only the transverse displacement due to bending rotations, the normal displacement of the bar at the interface can be predicted satisfactorily, as shown in later sections.

(5) Stresses, strains, and force system acting on embedded bar modeled as 2-D cord

From the assumed distributions of bond stress and curvature, computations can be carried out for the sectionally averaged mean bar stresses and strains along the bar axis ($\overline{\sigma}_s(x)$ and $\overline{\varepsilon}_s(x)$, respectively), the local stresses and strains over the bar cross section, ($\sigma_s(x,y)$ and $\varepsilon_s(x,y)$, respectively, where y is the local coordinate with an origin at the centroid of the section concerned), and the system of forces (including axial force P(x), bending moment M(x), shear force V(x), and contact pressure below the bar $f_b(x)$), along the bar axis. The discretized bar local stresses, $\sigma_s(x,y)$, are computed from the uniaxial stress-strain relationship of a bare steel bar[2]. Making use of the relationships between the mean axial bar stresses and strains with the local stresses and strains, we have,

$$\overline{\sigma}_s(x) = \frac{\int_{-D/2}^{D/2} \sigma_s(x,y)\,dA_s(y)}{A_s}, \qquad \overline{\varepsilon}_s(x) = \frac{\int_{-D/2}^{D/2} \varepsilon_s(x,y)\,dA_s(y)}{A_s} \tag{17}$$

where, D is the bar diameter. The governing equations are detailed below.

$$\overline{\sigma_s}(x) = \frac{4}{D}\int_0^x \tau_b(x)\,dx \tag{18}$$

$$where \quad \tau_b(x) = \tau_b(x, \tau_{b,\max}) \qquad (L_e - L_b \le x \le L_e)$$

which is the general equation obtained by integrating Eq.(2). The mean axial bar strain is then computed from $\overline{\sigma_s}(x)$ and $\phi(x)$ as,

$$\overline{\varepsilon}_s(x) = \overline{\varepsilon}_s(\phi(x), \overline{\sigma}_s(x)), \qquad L_e - L_b \le x \le L_e \tag{19}$$

$$where \quad \overline{\sigma_s}(x) = \int_{-D/2}^{D/2} \sigma_s(\varepsilon_s)\,dA_s(y)/A_s \quad and \quad \varepsilon_s = \overline{\varepsilon_s}(x) + \phi(x)\cdot y \tag{20}$$

The system of forces acting on the bar is then computed as below.

$$P(x) = \overline{\sigma}_s(x) A_s \tag{21}$$

$$M(x) = \int_{-D/2}^{D/2} \sigma_s(x,y)\cdot y\,dA_s(y) \tag{22}$$

$$V(x) = \frac{dM(x)}{dx} \tag{23}$$

$$f_b(x) = \frac{dV(x)}{dx}\cdot\frac{1}{D} \tag{24}$$

The effect of shear stress, τ_s, resulting from bending curvature on the yield stress of the bar is taken into consideration by applying the Von-Mises yield criterion, as below.

$$f_y'(x) = f_y\sqrt{1-3(\tau_s(x)/f_y)^2} \tag{25}$$

This yields the reduced mean yield stress, f'_y, used to check the fiber stress state of the bar.

By solving a) the bond constitutive model in Eq.(1-4) simultaneously with b) the compatibility conditions with respect to transverse shear displacement and force in Eq.(13-15) and c) the equilibrium of sectional forces in Eq.(17-25), we obtain the coupled effect of pullout and dowel actions. The spatial distribution of computed parameters obtained by simultaneously solving Eq.(1-5) and Eq.(13-24) along the bar axis are shown in **Fig.8**. Also shown is the profile of fiber stresses across the bar section in the 'Curvature Influenced Zone'.

(6) Ultimate axial force criterion for embedded bar

The ultimate axial force provided by the reinforcement under a coupled displacement path, which gives rise to interacting bending, shear, and axial forces on the embedded bar, can be derived on the basis of the maximum possible interactive stresses in the bar under such conditions. Using the plane section theory of beams, and idealizing the material stress-strain behavior as rigid plastic with a capacity equal to the bar axial yield capacity, the solution of two equilibrium conditions for a given cross section as described by Eq.(26) gives an interaction equation in terms of the ratios of actual forces to the strength of the section under pure axial and bending forces[13] as formulated in Eq.(27).

$$\int_{-D/2}^{D/2} \sigma_s(x,y)\,dA_s(y) = P(x), \qquad \int_{-D/2}^{D/2} \sigma_s(x,y)\cdot y\cdot dA_s(y) = M(x) \tag{26}$$

$$\frac{M(x)}{M_o}+\left(\frac{P(x)}{P_o}\right)^2=1 \tag{27}$$

Extending this relation to consider the effect of sectional shear forces according to the Von-Mises criterion for combined axial and shear forces, we obtain,

$$\lambda(x)=\left[\frac{M(x)}{M_o}+\left(\frac{P(x)}{P_o}\right)^2\right]^2+\left[\frac{V(x)}{V_o}\right]^2$$
$$\lambda(x)=1 \tag{28}$$

where M(x), P(x), and V(x) are the actual bending moment, axial force, and shear at a section, respectively; M_o ($=f_y D^3/6$), P_o ($=A_s f_y$), and V_o ($=A_s f_y/\sqrt{3}$) are the corresponding ultimate capacities under non-interactive force conditions. Under any combination of interacting stresses, when the limit criteria expressed by $\lambda(x)$ equals unity, the ultimate bar axial stress is implied unless there is a reduction in the other interactive forces.

The experimental verification for deriving an interaction failure criteria such as λ (x), based on plane section theory, is shown in **Fig.9**. Test results for the ultimate capacity of the section concerned, subjected to combined axial thrust and a bending moment[13] without instability problems, were analyzed using two different approaches. The first was the interaction criteria, as described above, and the second was by considering failure as occurring when the extreme bar fiber reaches fracture (as defined by the axial stress-strain relation of the bar,) under increasing bending moment and constant axial force. (Since the actual stress-strain relation of the steel section is not mentioned in reference (13), a typical relation for steel with similar yield stress was utilized[15].) It can be seen from **Fig.9** that satisfactory predictions of ultimate capacity can be obtained using the interaction criteria, whereas the second approach overestimates the data. Similar verification of the interaction equation for tests on hollow rectangular box sections subjected to a bi-axial moment and axial tension without instability problems can be found in reference (14).

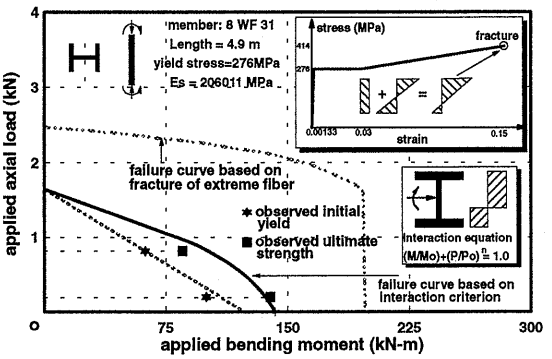

Fig.9 Interaction criteria with test results [13]

4. VERIFICATION OF PROPOSED MODEL

(1) Curvature-shear slip relation

Since the basic compatibility proposal in the model relates the curvature distribution with reinforcement shear slip, a comparison of experimentally measured and computed shear slips using Equation (13-15) and neglecting shear deformation (δ_{bs}=0), based on the experimentally obtained maximum bar curvature, is shown in **Fig.10** for some typical specimens. Satisfactory correlation can be identified despite considerable variation in maximum bar curvature for different specimens. This verification further confirms the earlier point that plastic shear deformation is not significant in coupled displacement path tests till the maximum bar axial capacity is attained.

(2) Bar axial stress-pullout relation at interface

Verification of bar stiffness and strength is done by testing reinforced crack and joint planes, as explained in the test setup shown in **Fig.1** for the introduction of a coupled displacement path for the embedded bar. Testing was carried out for different shear plane geometrical types (processed (P), and unprocessed (U), construction joints, CJ, and rough cracks, RC) and material properties (normal concrete, NC and self-compacting high performance concrete, HPC), along with different reinforcement ratios[16]. These define unique coupled displacement paths according to the equilibrium and compatibility conditions at the interface.

The measured and computed steel axial mean stresses versus pullout resistance and associated transverse displacement at the interface are shown in **Fig.11.** The mean axial stress versus strain results for a similar test specimen[1] at the maximum curvature location are shown in **Fig.12.** Pure axial pullout results are also shown for comparison in all the figures. The dotted line with an arrow head leading from the coupled path prediction in these figures represents the point at which the limiting interactive force criterion, $\lambda(x)$, attains unity. A further increase in displacement path would result in plastic deformation without an increase in the axial stress, since the bending moment does not decrease with increasing bar transverse displacement. The critical location along the bar axis where the limit interactive force criterion is attained is always the point of maximum curvature inside the concrete; this is the point of maximum bending moment and axial force and zero shear.

This results in the formation of a plastic hinge, since additional bending moment cannot be supported and a possible rotational mechanism develops in the bar between the maximum curvature location and the interface, resulting in loss of the axial restraining force at the interface.

The satisfactory correlation over the initial part of the steel stress-pullout relation (before localized yielding occurs), verifies the first premise of the model regarding the quantitative effect of the profile of the 'Bond Deterioration Zone'. This explains the increased pullout resistance, as compared to the uniaxial pullout capacity of the original model with bond deterioration suppressed.

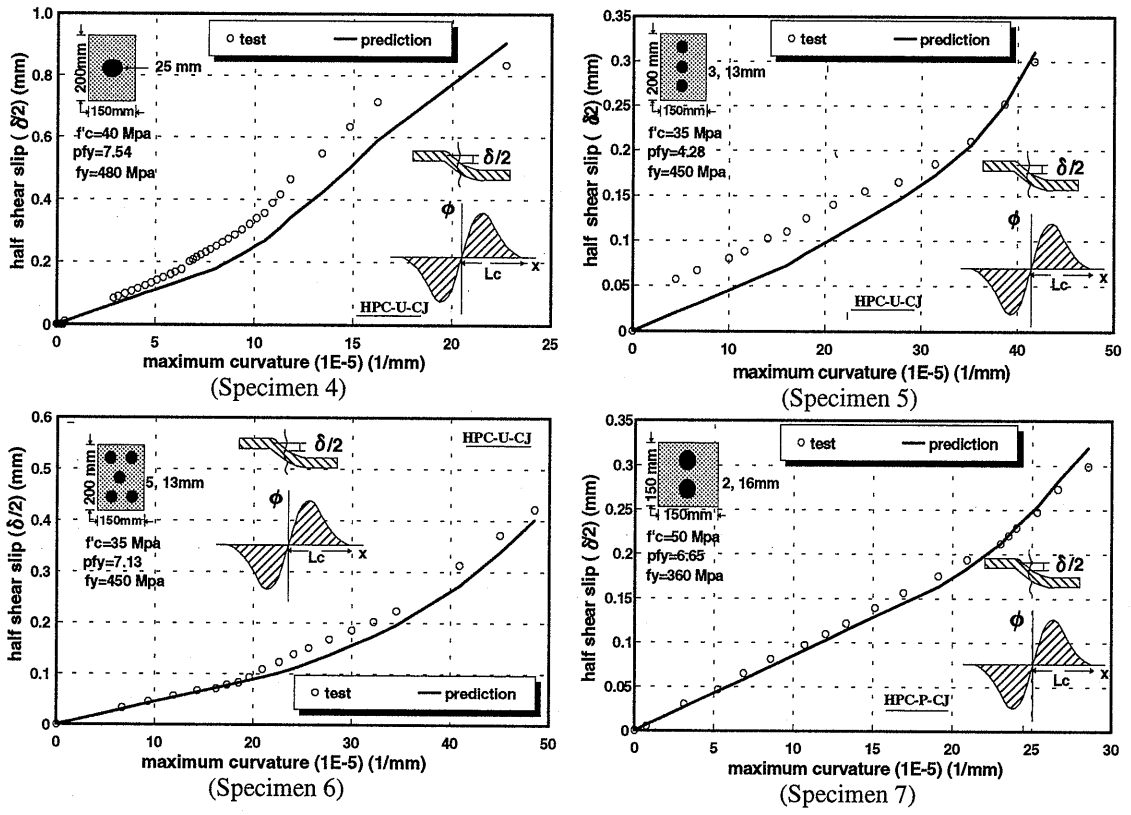

Fig.10 Comparison of experimental [16] and predicted results of compatibility relation between curvature and transverse displacement of bar for typical specimens

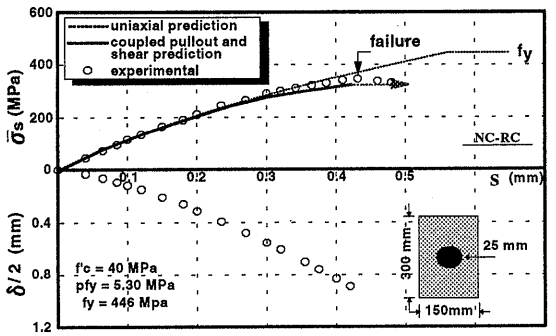

(Specimen 1)

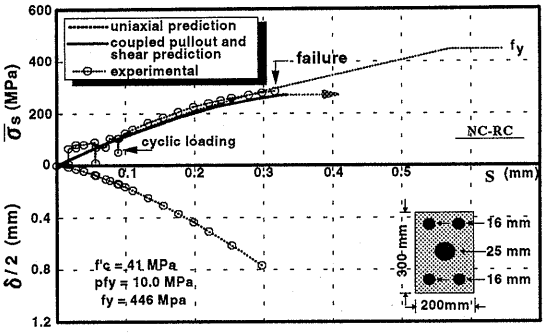

(Specimen 2)

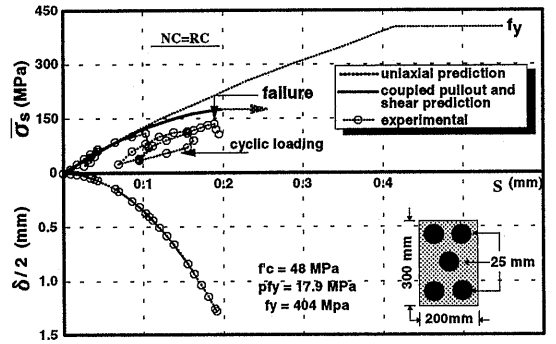

(Specimen 3)

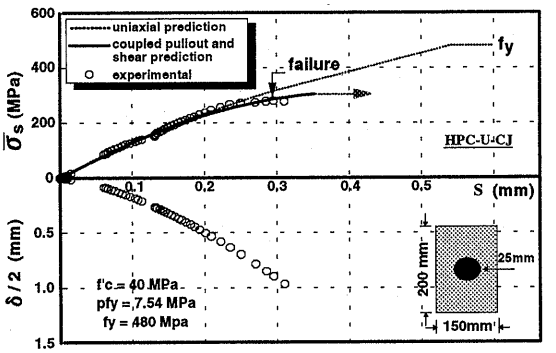

(Specimen 4)

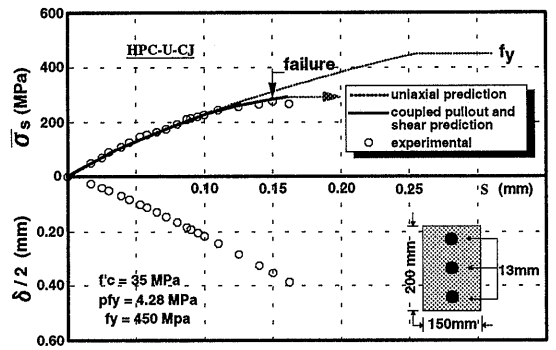

(Specimen 5)

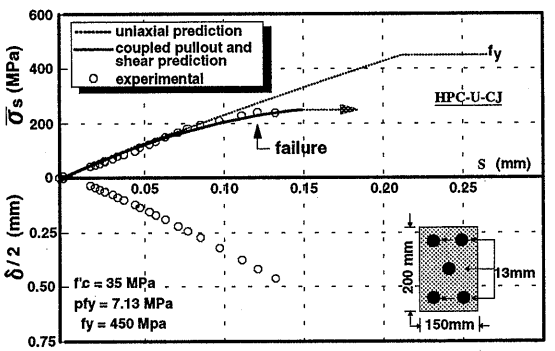

(Specimen 6)

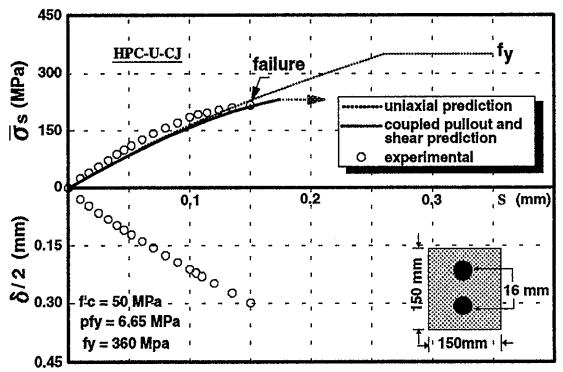

(Specimen 7)

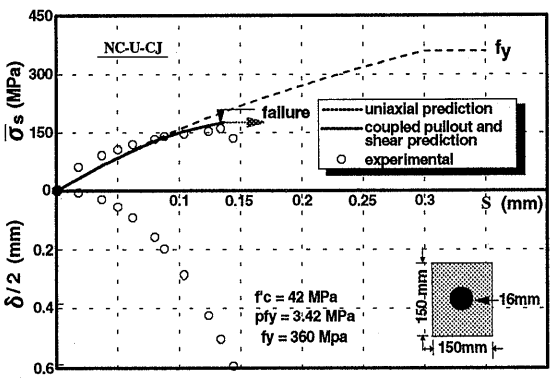

(Specimen 8)

Fig.11 Comparison of experimental [16] and predicted mean axial bar stress at specimen failure, and associated displacement path at the interface

After localized yielding of the extreme bar fibers, the mean strain profile becomes non-uniform as a result of the induced curvature, since the mean stress profile is uniform near the crack. Since the integral of mean strain along the bar represents the pullout of the bar, this non-uniformity in the mean strain profile is the source of the additional pullout for a given mean stress level observed in coupled displacement path tests as compared to uniaxial pullout tests. The correlation of the non-linear part of the steel stress-pullout relation verifies the second premise of the model regarding the quantitative effect of the 'Curvature Influenced Zone'. In consideration of the limiting value of the interactive stresses possible at the maximum curvature location due to combined axial and bending stresses, the ultimate axial force on the bar can also be predicted satisfactorily (See **Fig.11** and **Fig.12**).

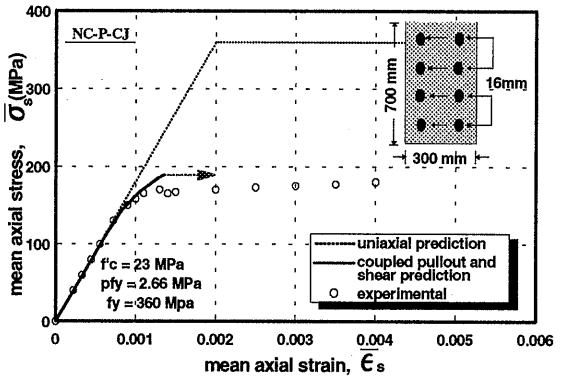

Fig.12 Comparison of experimental [16] and predicted sectionally averaged mean axial stress and strain at maximum curvature location [1]

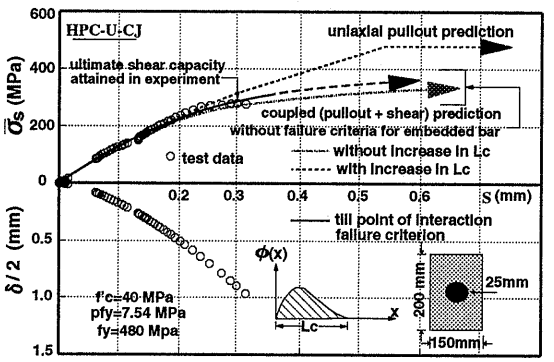

Fig.13 Comparison of experimental [16] and predicted mean bar axial stress with associated displacement paths without limiting failure criteria for bar

In general, the steeper the displacement path, brought about by increased reinforcement ratio, in terms of δ_b/S, the flatter the interface geometry, or the lower the concrete strength, then the lower the mean axial stress attained, as evident through **Fig.11** (Specimens 3,6,8, respectively).

In order to clearly understand the significance of the proposed model's interaction failure criterion introduced in Eq.(28), a typical test specimen is analyzed without considering any failure criteria for the bar other than fracture of the extreme fibers at the end of strain hardening. The results of this analysis are shown in **Fig.13**. Two cases, with and without consideration of an increase in curvature influenced zone, L_c, are computed so as to check the sensitivity of this proposal. It can be seen that if no failure criterion is defined, bar pullout continues to increase with small increase in axial stress, thereby reducing pullout stiffness.

Test results, however, do not indicate such high bar pullout values. On the other hand, the good correlation obtained with test data for both bar axial capacity and associated pullout at the interface in the case of coupled displacement paths with the interaction failure criterion means that this is an acceptable failure condition for the proposed model. The sensitivity of the simulation to an increase in L_c, as seen in **Fig.13**, indicates that relaxation of the supporting concrete spring properties reduces the rate of curvature increase at a particular location, and the bar axial stresses attained for a given pullout level are increased. However, till the point of observed bar capacity, the effect of the increase in L_c on the bar axial stress versus pullout relation is small.

(3) Force-displacement relationship of embedded bar under pure transverse load

The behavior of an embedded bar under a pure transverse load, termed dowel action, has been experimentally investigated by several researchers[4),6)]. The proposed generic model for an embedded bar can also be applied to cases of pure transverse displacement to predict dowel capacity and load displacement relationships. In the absence of any axial pullout, the nonlinearity in the bar under pure shear is much higher than in the case of a bar subjected to a coupled displacement path.

The failure mode is highly ductile with a large spread of plastic strain along the bar axis and large plasticized depths across the bar section. The presence of a zone of localized curvature is also known under such conditions[4)], similar to that seen in tests conducted in this study for coupled displacement paths. A comparison

of test [4] and predicted results for bars of different diameters is shown in **Fig.14**, showing good agreement.

Predictions are also attempted for test data from reference (9), with different bar diameters and different bar and concrete material properties from reference (4). The predictions obtained are again in good agreement with the test data, as shown in **Fig.14,** thus, verifying the versatility of the proposed bar model. Not only can it predict mean bar axial stress versus pullout behavior coupled with transverse displacement, but also bar shear stress versus transverse displacement in the absence of any axial pullout. Thus, the formulated two-dimensionally idealized generic bar model can be used to successfully predict axial and transverse bar behavior under any arbitrary coupled or uncoupled displacement path.

Since the validity of the bar model has been verified in a wide range of tests, it can be used to numerically simulate the effect of varying axial force on the reduction of dowel capacity, the possibility of which was raised by Suzuki et al.[11] Although test results in reference (11) show considerable scatter and higher dowel capacities than observed in other test results [4),9)], probably due to insufficient elimination of aggregate interlock, the qualitative trend of reduced dowel capacity with increasing axial force was observed. Computational results of dowel load-transverse displacement behavior in the presence of varying axial force are shown in **Fig.15**.

From the computed results, it is observed that under small axial force, the main source of stiffness degradation in dowel behavior is inelasticity of the supporting concrete due to increasing transverse displacement, which in turn induces higher bearing pressure. This becomes more and more severe in the presence of higher axial forces, and the stiffness degradation is accelerated. Under very high axial forces close to the axial capacity of the bar, the limit condition of maximum interactive stresses governs the ultimate dowel capacity.

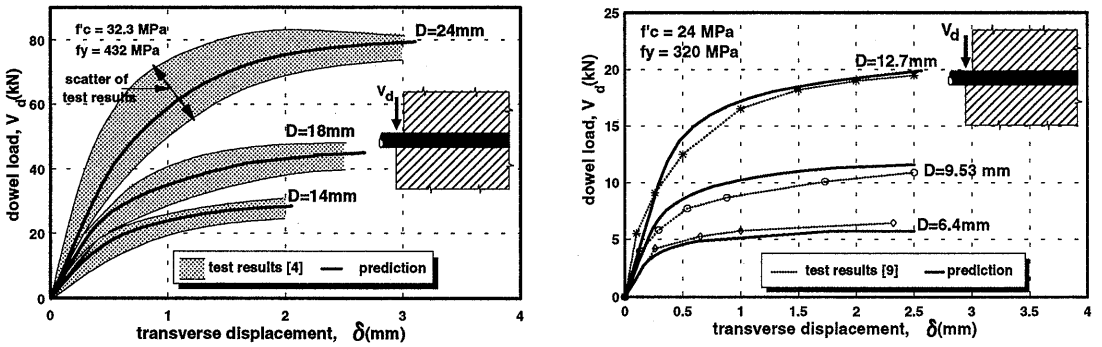

Fig.14 Correlation of dowel load-displacement relation in test results [4), 9)]

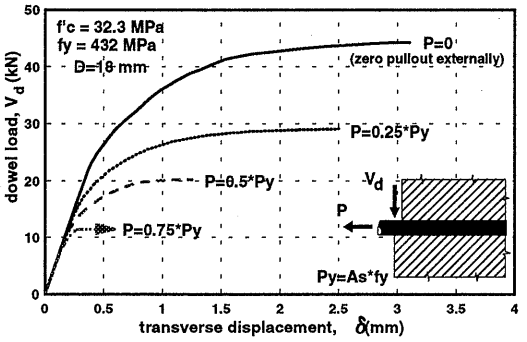

Fig.15 Effect of axial force on dowel load-displacement behavior (computation)

5. CONCLUSIONS

Based on new experimental findings related to microscopic bar behavior derived from the mechanics of a RC interface, a generic model for embedded bars has been formulated. The model formulation follows rational micro and macro concepts and verifications were conducted using test data for each governing step. The

following are the general conclusions reached within the scope of this work:

1) By making two basic proposals based on experimental results, a 'Bond Deterioration Zone' and a 'Curvature Influenced Zone', and adopting a compatibility relation to predict curvature from transverse displacement, the internal stresses and strains (both along the bar axis and across its section) along with the entire system of forces acting on a bar embedded in concrete can be computed when subjected to coupled pullout and transverse shear slip.

2) The compatibility relation between bar curvature and normal bar displacement can be established using the in-plane hypothesis of sections and predicting transverse shear displacement of the bar from its curvature distribution, and this is verified using experimental results.

3) The reduced axial stiffness of the bar can be computed from the initiation of localized plasticity in the reinforcing bar inside concrete, even if the section at the interface is in a purely elastic state. The progressive reduction in axial stiffness due to gradually increasing plasticity both along the bar axis and across the bar section with increasing shear displacement can be predicted.

4) The maximum axial confining stress attained in the reinforcing bar at the interface can be predicted by considering the ultimate interactive stress possible at the maximum curvature location due to combined axial and bending stresses.

5) The proposed model can also predict the capacity and load-displacement behavior of an embedded bar under a pure transverse displacement path. This makes the model a generic one applicable to any displacement path, including pure axial pullout, pure transverse displacement, or any arbitrary combination of the two.

6) The proposed model has been independently verified with displacement paths obtained by experiments and used as input parameters. For versatile applicability, predictions of the stress transfer behavior of a RC interface by combining this proposal with an aggregate interlock model is necessary. Since the evaluation of shear force acting on the bar at the interface, i.e. dowel shear, can be computed from the model, it can be added to the aggregate interlock model to obtain the total shear transferred at the interface by both mechanisms in a unified manner.

In future development, the proposed model should be extended to cover more generic conditions in reinforced concrete members, such as dense arrangements of reinforcing bars, and adjacent cracks with small spacing, etc.

REFERENCES

1) Maekawa, K., Mishima, T., Khan, J. and Qureshi, J.: Reduced Axial Stiffness of Deformed Bars Under Shear Slip Along Crack in Concrete, *CEB Conference, 'Bond in Concrete'*, 1993

2) Shima, H., Chou, L. and Okamura, H.: Micro and Macro Model for Bond Behavior in Reinforced Concrete, *Journal of the Faculty of Engineering, University of Tokyo (B),* Vol. 39, No.2, 1987

3) Bujadham, B., Maekawa, K. and Mishima, T.: Cyclic Discrete Crack Modeling for Reinforced Concrete, *Computer Aided Analysis and Design of Reinforced Concrete Structures*, Pineridge Press, pp. 1225-1236, 1990

4) Poli, S. D., Prisco, M. D. and Gambarova, P. G.: Shear Response, Deformation, and Subgrade Stiffness of a Dowel Bar Embedded in Concrete, *ACI Structural Journal*, V. 89, No. 6, pp.665-675, 1992

5) Mishima, T., Yamada, K. and Maekawa, K.: Localized Deformational Behavior of a Crack in RC Plates Subjected to Reversed Cyclic Loads, *Proceedings of JSCE*, No. 442/V-16, pp.161-170, 1992

6) Sourishian, P., Obaski, K., Rojas, M. C. and Sim, J.: Analysis of Dowel Bars Acting Against Concrete Core, *ACI Journal*, Proceedings V.83, No. 4, pp.17-42., 1986

7) Ueda, T., Lin, I. and Hawkins, N. M.: Beam Bar Anchorages in Exterior Column Beam Connections, *ACI Journal*, pp.412-422, 1986

8) Tani, S.: Inelastic Analysis of R/C Frame Structures, *Proceedings of ASCE*, Vol. 100, ST7, pp.1433-1449, 1974

9) Paulay, T., Park, R. and Phillips, M. H.: Horizontal Construction Joints in Cast-In-Place Reinforced Concrete, Shear in Reinforced Concrete, *ACI Publication SP* 42-27, Vol.2, pp. 599-616, 1974

10) Izumo, J., Shima, H. and Okamura, H.: Analytical Models for RC Panel Elements Subjected to In-Plane Forces, *Concrete Library of JSCE*, No. 12, pp. 155-181, 1989

11) Suzuki, M., Nakamura, T., Horiuchi, M. and Ozaka, Y: Experimental Study on the Influence of Tension Force on Dowel Effect of Axial Bars, *Proceedings of the JSCE*, No. 426/V-14, pp. 159-166, 1991 (In Japanese)

12) Okamura, H. and Maekawa, K.: *Nonlinear Analysis and Constitutive Models of Reinforced Concrete*, Gihodo-Press, Tokyo, 1991

13) Beedle, S. L., Ready, J. A. and Johnston, B. G.: Tests of Columns Under Combined Thrust and Moment, *Proceedings of Society of Experimental Stress Analysis*, Vol. 8, pp. 109-132, 1950

14) Khalil, H. S. and Tadros, G. S.: Plastic Resistance of Mild Steel Rectangular Sections, *The Structural Engineer*, No. 7, Vol. 51, pp. 239-249, 1973

15) Park, R. and Paulay, T.: *Reinforced Concrete Structures*, Wiley Interscience Publication, pp. 38, 1975

16) Maekawa, K. and Qureshi, J.: Embedded Bar Behavior in Concrete Under Combined Axial Pullout and Transverse Displacement, *Proceedings of JSCE*, No.532/V-30, pp.183-195, 1996